ELSEVIER

Journal of Nuclear Materials 278 (2000) 212–224

journal of nuclear materials

www.elsevier.nl/locate/jnucmat

XAS and XRD study of annealed ^{238}Pu- and ^{239}Pu-substituted zircons ($Zr_{0.92}Pu_{0.08}SiO_4$)

B.D. Begg [a], N.J. Hess [b], W.J. Weber [b,*], S.D. Conradson [c], M.J. Schweiger [b], R.C. Ewing [d]

[a] *Australian Nuclear Science and Technology Organisation, PMB 1, Menai, NSW 2234, Australia*
[b] *Pacific Northwest National Laboratory, PO Box 999, MSIN K2-44, Richland, WA 99352, USA*
[c] *Los Alamos National Laboratory, Los Alamos, NM 87545, USA*
[d] *Department of Nuclear Engineering and Radiological Sciences, University of Michigan, Ann Arbor, MI 48109, USA*

Received 1 June 1999; accepted 29 September 1999

Abstract

An annealing study has been completed on two compositionally identical Pu-substituted zircons ($Zr_{0.92}Pu_{0.08}SiO_4$) prepared 18 yr ago with different ^{238}Pu/^{239}Pu isotopic ratios. The activity and accumulated dose for each material varies greatly due to the very different half-lives of ^{238}Pu (87.7 yr) and ^{239}Pu (24 100 yr). The predominantly ^{238}Pu-substituted zircon is in a highly amorphous state after accumulating a dose of 2.8×10^{19} α-decays/g, which is a factor of two higher than the dose previously determined necessary to amorphize this material. The ^{239}Pu-substituted zircon has remained highly crystalline after an accumulated dose of 1.2×10^{17} α-decays/g. The Pu in both samples is trivalent due to sintering under reducing conditions. The short-range and long-range structures of each sample have been characterized by detailed X-ray absorption spectroscopy and X-ray diffraction (XRD) methods. The oxidation of Pu^{3+} to Pu^{4+} in the crystalline ^{239}Pu-substituted zircon during annealing in air resulted in a decrease in lattice distortion due to the decrease in ionic radius of Pu^{3+} to Pu^{4+} on the Zr^{4+} site. A significant amount of PuO_2 exsolved from the zircon structure after annealing at 1200°C in air. Detailed characterization of the amorphous ^{238}Pu-substituted zircon demonstrated that while devoid of long-range order it still retained a distorted zircon structure and composition over a length scale of 0.5 nm. The recrystallization of the amorphous ^{238}Pu-substituted zircon could be achieved directly at temperatures as low as 1200°C when annealed for 12 h in air; however, annealing at 1000°C resulted in decomposition into constituent oxides.

PACS: 61.10.Ht; 61.10.Nz; 61.43.Er; 61.80.-x; 61.82.Ms

1. Introduction

One of the principal factors that will determine the long-term durability of nuclear waste forms proposed for the immobilization of high-level radioactive waste or actinide-rich waste is the structural response to self-radiation damage as a function of time and temperature. This is especially true for waste forms designed to incorporate actinide elements, such as plutonium, because they will be subject to considerable self-radiation damage from α-decay events [1,2]. With this in mind, an accelerated study of α-decay damage was initiated 18 yr ago to investigate self-radiation effects from α-decay in ^{238}Pu-substituted zircon, $ZrSiO_4$, and compare the results with data on natural zircons. The detailed results of damage accumulation and recovery from the initial phase of this study have been reported previously [3–6].

Although the initial study focused primarily on ^{238}Pu-substituted zircon, two types of synthetic zircons were

* Corresponding author. Tel.: +1-509 375 2299; fax: +1-509 375 2186.
E-mail address: bill.weber@pnl.gov (W.J. Weber).

0022-3115/00/$ - see front matter
PII: S0022-3115(99)00256-1

actually prepared, one containing a mixture of 8.85 wt% ^{238}Pu and 1.15 wt% ^{239}Pu and the other containing 10 wt% ^{239}Pu. In both instances, the Pu was substituted directly for Zr, giving a $Zr_{0.92}Pu_{0.08}SiO_4$ stoichiometry. Initial characterization by X-ray diffraction (XRD), found both samples to be single-phase zircons. The first zircon containing 8.85 wt% ^{238}Pu, with its 87.7 yr half-life, provided a means of accelerating the α-decay rate (i.e., damage rate) by a factor of ~250 when compared to the sample containing 10 wt% ^{239}Pu. This ^{238}Pu-substituted zircon became amorphous to XRD analysis after a dose of 0.7×10^{19} α-decays/g [3,5]. Details of the sample preparation procedures and the initial characterization have been reported previously [3–6]. Self-heating in the ^{238}Pu-substituted zircon specimens during storage is minimal, and specimen temperatures have been estimated to be less than 50°C.

These zircon samples have been more recently characterized by X-ray absorption spectroscopy (XAS) after accumulated doses of 2.8×10^{19} and 1.2×10^{17} α-decays/g for the ^{238}Pu- and ^{239}Pu-substituted zircons, respectively [7,8]. The ^{238}Pu-substituted zircon in these studies achieved a dose that is a factor of two higher than that determined necessary to fully amorphize the same samples [3–6]. The XAS results [7,8] confirmed that self-radiation damage had transformed the ^{238}Pu-substituted zircon into a fully amorphous state lacking long-range order. Surprisingly, the Pu L_{III}-edge XANES indicated that the Pu in both zircon samples was completely trivalent. This was an unexpected result of originally preparing the Pu-substituted zircons under a reducing atmosphere (oxygen-purged flowing argon). The trivalent state of Pu in zircon poses a number of questions, notably how is Pu^{3+} incorporated into the zircon structure, due to the apparent significant ionic radii mismatch between Pu^{3+}, 0.100 nm (sixfold coordination [9]) and Zr^{4+}, 0.084 nm (eightfold coordination [9]), and consequently how has charge neutrality been maintained? Although it is preferable to compare the ionic radii of Pu^{3+} and Zr^{4+} on equivalently coordinated sites, the ionic radius of Pu^{3+} in eightfold coordination corresponding to the Zr^{4+} site in zircon is unknown. Recent computer simulations, however, using energy minimization techniques [10] indicate that the lowest energy configuration occurs for a defect cluster composed of two near-neighbor Pu^{3+} substitutions on Zr^{4+} sites and a neighboring charge-compensating oxygen vacancy.

In order to further understand the behavior of Pu in zircon and recrystallization processes, an annealing study was undertaken with the twofold aim of oxidizing (in air) the Pu^{3+} to Pu^{4+} in both the amorphous (^{238}Pu-substituted) and crystalline (^{239}Pu-substituted) zircons, as well as to examine the nature of the recrystallization processes in the amorphous state of zircon. The original goal was to oxidize the Pu^{3+} in the amorphous zircon at a sufficiently low temperature to avoid any recrystallization.

There have been several previous isochronal annealing studies on zircons that are relevant to the present study. One of these studies [3,5,6] was carried out on the same ^{238}Pu-substituted zircon as in the current study but at a lower dose (1.35×10^{19} α-decays/g) where this zircon is first observed to be fully amorphous. Other studies have been carried out on natural metamict zircons [11–17]. Since zircon undergoes a large (~18%) volume expansion upon amorphization [3–6], the isochronal recovery processes in ^{238}Pu-substituted zircon [3,5,6] and in natural metamict zircon [11] were monitored via density measurements, as shown in Fig. 1. In each of these studies, a single specimen was sequentially annealed to successively higher temperatures. After each heat treatment, the sample's density was determined, and the structure was monitored by XRD methods or in some instances by optical spectroscopy. The first stage of the two-stage density recovery process is consistent with the initial crystallization of zircon's component oxides and would account for the observed 55–60% recovery of the density in both studies. The second stage of the density recovery process, which occurs above 1200°C, has been only observed in the ^{238}Pu-substituted zircon [3,5,6] and represents the recrystallization of the zircon structure, which was complete at 1450°C. Although the second stage of the density recovery process in the natural metamict zircon was not observed due to a restricted maximum temperature [11], Vance and Anderson [18] have reported the recrystallization of the zircon structure in another natural metamict zircon at 1300°C. The isochronal density recovery curves from the two studies (Fig. 1) are in good agreement with each other and consistent with the recovery of the integrated neutron diffraction intensity in natural metamict zircon [14]. The lower onset temperature for recovery that is

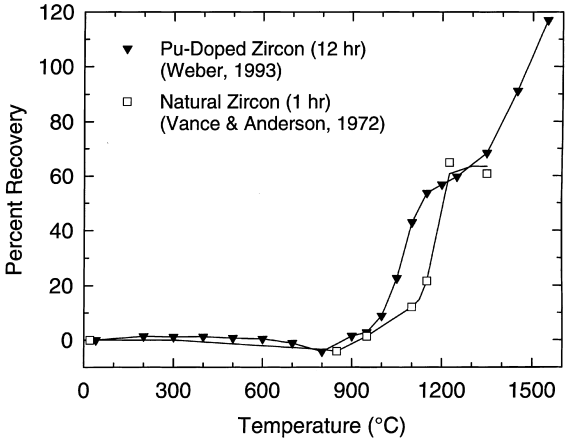

Fig. 1. Summary of isochronal density recovery studies of amorphous zircons by Weber [3,5,6] and Vance and Anderson [11].

observed for the ^{238}Pu-substituted zircon occurs because a 12 h isochronal period was used in the annealing of the ^{238}Pu-substituted zircon, while only a 1 h isochronal period was used for the metamict zircons. In the natural metamict zircon, Vance and Anderson [11] noted the development of diffuse diffraction maxima associated cubic zirconia after annealing at 850°C. By 1100°C, the diffuse pattern converted to the sharp diffraction pattern of tetragonal zirconia. At temperatures greater than 1150°C, the intensity of the tetragonal zirconia peaks decreased, although no evidence for zircon was observed in the powder XRD pattern at the maximum temperature of 1350°C. However, diffuse streaks in a Laue diffraction pattern, which had the symmetry of zircon, were observed after annealing at 1350°C. In the ^{238}Pu-substituted zircon [3,5,6], the appearance of cubic zirconia was first noted after annealing at 1050°C.

In light of these previous studies, the amorphous ^{238}Pu-substituted zircon was annealed at 1000°C for 12 h in air. This temperature represented a compromise between being sufficiently high enough to ensure complete oxidation of the Pu^{3+} and low enough to avoid recrystallization. A second ^{238}Pu-substituted zircon specimen was annealed at 1200°C for 12 h in air in order to study the recrystallization of the amorphous zircon in the transition region of the two-stage recovery process. In addition, the crystalline ^{239}Pu-substituted zircon was annealed at 1200°C for 12 h in air in order to oxidize the Pu^{3+}. In these annealing studies, the heating rate was on the order of 600°C/h.

2. Experimental

The original preparation of the ^{238}Pu- and ^{239}Pu-substituted zircon samples used in this study has been described previously [3,5,6]. The high-temperature anneals were carried out on small (~1 g) solid specimens that were subsequently ground into powder, mixed with colloidion-amyl acetate solution, and loaded as a slurry into aluminium holders with Kapton windows.

EXAFS and XRD measurements were performed at the Stanford Synchrotron Radiation Laboratory. EXAFS spectra were collected at the Pu L_{III}- and Zr K-edges in transmission and fluorescence modes simultaneously out to a photoelectron wavevector of 1.3 nm^{-1} at 77 K. The transmission spectra were measured with standard ionization chamber detectors, while the fluorescence was recorded with a 13-element Ge detector. Energy calibration was performed by assigning the first inflection point in the absorption edge of a Zr foil to 17,999.35 eV. Data analysis was performed in a standard manner that has been described previously [7,8].

The XRD spectra were collected in transmission out to a maximum of ~2 nm^{-1} in reciprocal space using monochromatic X-rays of energy between 20–30 keV, at 77 K. A solid-state detector coupled to a digital amplifier, which provided an energy spectrum at every point in the pattern that is analyzed by the data acquisition software, was used to measure the diffracted beam intensity, as well as the sample's fluorescence that enabled volume corrections to be made. The intensity of the incident beam was also monitored with an ionization chamber to provide for normalization. Pair distribution function analysis of the diffraction pattern was carried out using PDF 1.00 software [19,20].

3. Results

3.1. ^{239}Pu-substituted zircon annealed at 1200°C for 12 h in air

Pu L_{III}-edge XANES revealed that annealing the ^{239}Pu-substituted zircon at 1200°C for 12 h in air was sufficient to fully oxidize the Pu^{3+} to Pu^{4+}. XRD indicated, however, that as a result of this heat treatment the sample now contained a considerable amount of PuO_2 in addition to zircon. This was quite unexpected given that the unannealed ^{239}Pu-substituted zircon was single phase, and the Pu L_{III}-edge EXAFS had indicated that the Pu was uniformly distributed within the zircon lattice, which excluded the possibility of any amorphous Pu-bearing second phases in the unannealed zircon [7,8]. Therefore, the PuO_2 observed in the annealed ^{239}Pu-substituted zircon appears to have been exsolved from the zircon lattice as a result of this 1200°C heat treatment. The lattice parameters obtained from the zircon before and after annealing are compared in Table 1, along with the published reference values for zircon [21].

As expected, the unannealed ^{239}Pu-substituted zircon, in which the Pu was completely trivalent and contained

Table 1
A comparison of the unit cell volumes obtained from the ^{239}Pu-substituted zircon before and after annealing at 1200°C for 12 h in air with those for a reference zircon [21]

	^{239}Pu-zircon	^{239}Pu-zircon 1200°C/12 h	$ZrSiO_4$ [21]
Cell volume (nm^3)	0.2678	0.2623	0.2608
Δ rel. $ZrSiO_4$	+0.0070	+0.0015	0
Pu valence	+3	+4	–
Ionic size (nm)	0.100 (Pu)	0.086 (Pu)	0.072 (Zr)
% Pu in zircon	100%	50%	0%

in the zircon structure, had the largest unit-cell volume. The oxidation of the Pu^{3+} to Pu^{4+} combined with the exsolution of Pu from the annealed ^{239}Pu-substituted zircon lattice considerably reduced its unit-cell volume. A first-order estimate of the amount of Pu exsolved from the annealed ^{239}Pu-substituted zircon may be made, based on the measured unit-cell volumes and the differences in ionic radii between Pu^{3+}, Pu^{4+} and Zr^{4+}, as outlined in Table 1. Since the difference in ionic radii between Pu^{3+} and Zr^{4+} is twice that between Pu^{4+} and Zr^{4+}, it would be expected that, relative to the reference zircon, the increase in unit-cell volume for a given amount of Pu^{3+} substituted on the Zr^{4+} site should be approximately twice that for Pu^{4+}. Given that the measured difference in the unit-cell volume of the annealed ^{239}Pu-substituted zircon, relative to the reference zircon, is only ~43% of that expected, the annealed ^{239}Pu-substituted zircon is estimated to contain ~43% of the Pu. Recent Mean Field calculations [10], however, have predicted that the increase in lattice volume associated with the substitution of an equivalent amount of Pu^{3+} instead of Pu^{4+} on the Zr^{4+} site would be a factor of 1.8 rather than 2, as used here. Based on this value, the amount of Pu retained in the zircon is estimated to be ~48%. A number of other factors also influence the unit-cell volumes that have not been taken into account in this first order approximation. These include the presence of oxygen vacancies, which would be the most likely means of charge compensating for the presence of Pu^{3+} on the Zr^{4+} site in the unannealed ^{239}Pu-substituted zircon, and radiation damage induced expansion of the unit cell. The later effect has, however, been shown to be almost insignificant for the low dose, 1.2×10^{17} α-decays/g, experienced by the ^{239}Pu-substituted zircon [5]. In light of the uncertainty in both the measurements and the calculations, it would be safe to conclude that the annealed ^{239}Pu-substituted zircon only contains approximately half of the original 0.08 formula units of Pu.

A comparison of the Fourier transforms of the Pu L_{III}-edge EXAFS collected before and after annealing is shown in Fig. 2. The presence of a significant amount of PuO_2 is clearly evident after the oxidizing anneal that has resulted in the large increase in the intensity of many of the transform features. In addition to the contribution from PuO_2, there is also an increase in the intensity of the resolvable Pu–Si shell from the zircon. An increase in the modulus of the Pu–Si feature in the transform indicates that the level of distortion associated with the presence of Pu in the zircon is reduced after the oxidizing anneal. This is expected given the reduction in the ionic size mismatch associated with the oxidation of the Pu^{3+} to Pu^{4+} on the Zr^{4+} site and the filling of the closely associated oxygen vacancy site. This decrease in the level of distortion may also be partly associated with the annealing of any irradiation-induced defects that may have been created at this low dose level.

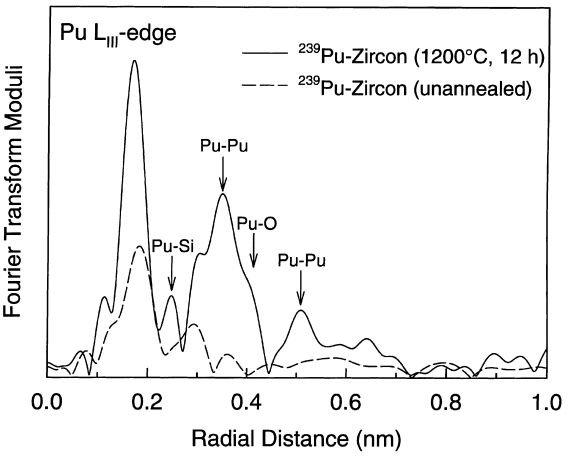

Fig. 2. Fourier transforms of the Pu L_{III}-edge EXAFS taken from the ^{239}Pu-substituted zircon before and after annealing in air at 1200°C for 12 h. Note that peaks in the Fourier transform have not been corrected for phase shift and as a result appear 0.05–0.10 nm shorter than fitted values.

A comparison of the Pu L_{III}-edge EXAFS fitting results obtained from the ^{239}Pu-substituted zircon before and after annealing, is shown in Table 2. The Pu environment in the unannealed ^{239}Pu-substituted zircon is well described by the $PuSiO_4$ standard [22], which would suggest that the Pu^{3+} present in the unannealed ^{239}Pu-substituted zircon has substituted on the Zr^{4+} site as planned, despite the large ionic size mismatch. Charge compensation has most likely occurred through the presence of an appropriate number of oxygen vacancies, giving the zircon $[Zr_{0.92}Pu_{0.08}]Si[O_{3.96}\square_{0.04}]$ stoichiometry. This is consistent with recent theoretical defect calculations [10] that indicated that the energy cost associated with placing Pu^{3+} in an interstitial position is five times that for placing it on the Zr^{4+} site. In addition, the calculations predict that the defect energy can be reduced by a further factor of four, if the Pu^{3+} forms clusters consisting of two Pu^{3+} on near-neighbor Zr^{4+} sites and an oxygen vacancy for charge compensation. No evidence for Pu clustering (i.e., as PuO_2) was observed in the Pu L_{III}-edge EXAFS from the unannealed ^{239}Pu-substituted zircon.

As indicated by the Fourier transform, PuO_2 dominated the fit to the Pu L_{III}-edge EXAFS from the annealed ^{239}Pu-substituted zircon. After the anneal, the intensity of the resolvable Pu–Si shell both increased and appeared at a significantly shorter distance, which would be expected given the reduction in ionic size associated with the oxidation of Pu^{3+} to Pu^{4+}.

A comparison of the local Zr environments from the ^{239}Pu-substituted zircon before and after annealing at 1200°C in air is shown in Fig. 3. The Fourier transforms of the Zr K-edge EXAFS indicate good structural

Table 2
A comparison of the Pu L_{III}-edge EXAFS fitting results for the ^{239}Pu-substituted zircon before and after being annealed at 1200°C for 12 h in air. Also shown are reference data from $PuSiO_4$ [22] and PuO_2 [29]

	Shells	Pu–O	Pu–O	Pu–Si	Pu–Si/Zr	Pu–O
^{239}Pu-zircon	Distance (nm)	0.221 (2)	0.239 (2)	0.316 (2)	0.364 (2)	0.415 (2)
	Number	2.9 (8)	5 (1)	1.0 (3)	7 (2)	3 (1)
	Δ Sigma	0.00	0.00	0.07 (2)	0.14 (2)	0.00
$PuSiO_4$	Distance (nm)	0.229	0.249	0.311	0.378	0.421
	Number	4	4	2	4/4	8
	Shells	Pu–O	Pu–Si	Pu–Pu	Pu–O	Pu–Pu
^{239}Pu-zircon 1200°C/12 h	Distance (nm)	0.230 (2)	0.300	0.387 (1)	0.438 (2)	0.532 (2)
	Number	7 (2)	1.6 (5)	6 (1)	23 (6)	3 (1)
	Δ Sigma	0.08	0.07	0.02	0.03	0.00
PuO_2	Distance (nm)	0.234		0.382	0.447	0.539
	Number	8		12	24	6

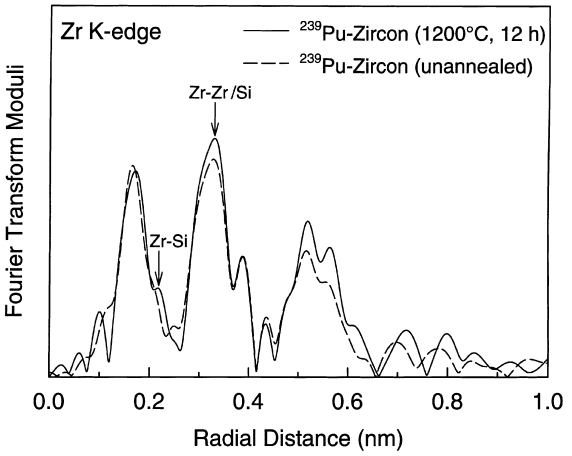

Fig. 3. Fourier transforms of the Zr K-edge EXAFS taken from the ^{239}Pu-substituted zircon before and after annealing in air at 1200°C for 12 h. Note that peaks in the Fourier transform have not been corrected for phase shift and as a result appear 0.05–0.10 nm shorter than fitted values.

agreement out to ~0.65 nm, beyond which deviations exist. Having said that, a significant difference is present in the region of ~0.25 nm, where the first resolvable Zr–Si distances reside. The effect of the oxidation of the Pu^{3+} to Pu^{4+}, and the accompanying reduction in lattice distortion, is therefore clearly evident on the neighboring Zr sublattice through changes in the first Zr–Si correlation, which appears very sensitive to structural distortion in the zircon. Zircon is composed of chains of alternating edge-sharing ZrO_8 polyhedra and SiO_4 tetrahedra that are cross-linked through corner-sharing SiO_4 tetrahedra. The first Zr–Si correlation at 0.299 nm arises from edge-sharing ZrO_8 polyhedra and SiO_4 tetrahedra; whereas, the Zr–Si correlation at 0.366 nm results from corner sharing polyhedra and tetrahedra. The reduction of the first Zr–Si correlation in the unannealed ^{239}Pu-substituted zircon may indicate disruption of some edge-sharing relationships, formation of some corner-sharing configurations by the rotation of SiO_4 tetrahedra away from the ZrO_8 polyhedra, and creation of some oxygen vacancies for the charge compensation of the Pu^{3+}.

The extent of atom pair correlations was determined by taking the Fourier transform of the corrected diffraction pattern to give a pair distribution function (PDF). The PDF shows the probability of finding two atoms a distance r apart weighted by the product of their atomic numbers. Comparisons of the PDF patterns taken before and after annealing are shown in Fig. 4. While the common features of zircon are clearly evident, the PDF features from the annealed ^{239}Pu-substituted

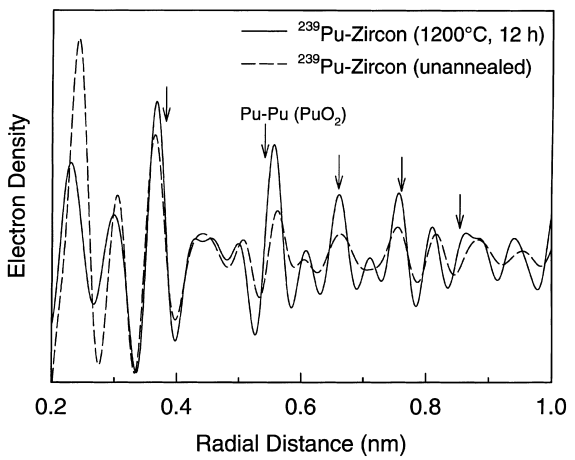

Fig. 4. Pair distribution function obtained from the ^{239}Pu-substituted zircon before and after annealing in air at 1200°C for 12 h. The positions of the dominant Pu–Pu pairs from PuO_2 are indicated by arrows.

zircon are significantly sharper and more intense than those from the unannealed ^{239}Pu-substituted zircon, reflecting the significant reduction in lattice distortion associated with the oxidation of the Pu^{3+} to Pu^{4+} and recovery of dilute damage from the relatively small α-decay dose. The intensity variations seen in the PDF data are consistent with those observed in the Fourier transforms from the Pu and Zr environments described above and reflect the complementary nature of these independent measurements. The presence of PuO_2 in the annealed ^{239}Pu-substituted zircon was also evident, as indicated by the location of the dominant Pu–Pu pairs from PuO_2 in Fig. 4.

3.2. ^{238}Pu-substituted zircon

Prior to discussing the annealing studies on the amorphous ^{238}Pu-substituted zircon, it is important to review the earlier XAS finding [7,8] in light of more recent XRD results. Fig. 5 shows a normalized coherent diffraction pattern obtained from the ^{238}Pu-substituted zircon using high-brightness synchrotron radiation. The very broad diffuse nature of the diffraction pattern is consistent with the lack of long-range order in the zircon. Superimposed on the amorphous background, however, is a very small amount of PuO_2, which is estimated to be less than 1% of the total Pu present in the sample. This was most likely present in the starting material but, due to its low concentration, was not detectable above the initial crystalline zircon background with the laboratory-source XRD unit used in the initial study [3]. The presence of such a small proportion of PuO_2 is also not irreconcilable with the earlier Pu L_{III}-edge XANES findings that indicated that all the Pu was trivalent due to the limited sensitivity of the technique.

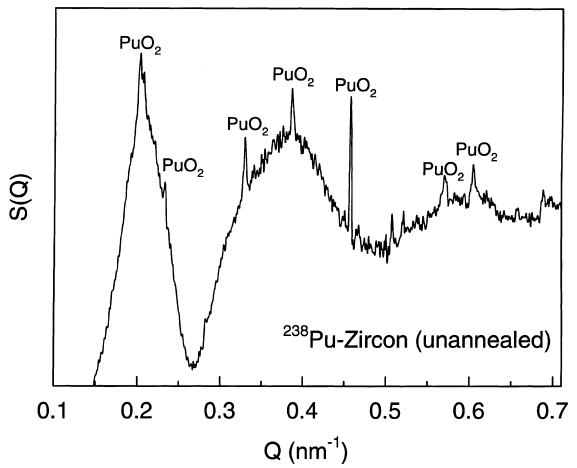

Fig. 5. Corrected XRD pattern from the amorphous (unannealed) ^{238}Pu-substituted zircon, showing a small amount of PuO_2.

PDF analysis of this diffraction pattern was undertaken to look for evidence of short-range order in this otherwise amorphous material, and the results are shown in Fig. 6. Also shown is a fit to the data based on crystalline zircon to which a broadening component has been added to simulate lattice distortion. Despite its amorphous state, there appears to be excellent agreement between the data and the distorted zircon fit out to a distance of ~0.5 nm, after which the long-range zircon structure appears to have been lost. The two minor peaks in the PDF at ~0.66 nm and ~0.85 nm coincide with the Pu–Pu distances in PuO_2, indicated in Fig. 6. A detailed breakdown of the cation pairings that constitute the fit out to ~0.5 nm, also shown in Fig. 6, indicates that despite the loss of long-range crystallinity a distorted zircon structure remains over a length scale of about 0.5 nm. This is consistent with the retention of the first Zr–Zr and Si–Si pairs. The first Zr–Si pairs at ~0.3 nm appear to have been lost, which suggests a complete loss of the edge-sharing relationships and the rotation of the SiO_4 tetrahedra away from the ZrO_8 polyhedra in the amorphous state, as suggested by Farges and Calas for metamict natural zircon [23] and similar to that proposed for cation polyhedra in natural metamict zirconolite [24]. The fit also suggests that the main Zr–Zr correlation has contracted to a slightly shorter distance, which is consistent with previous EXAFS results on these samples [7] and on natural metamict zircons [15,23].

The local Pu environment in this sample was characterized with Pu L_{III}-edge EXAFS, and the fitting

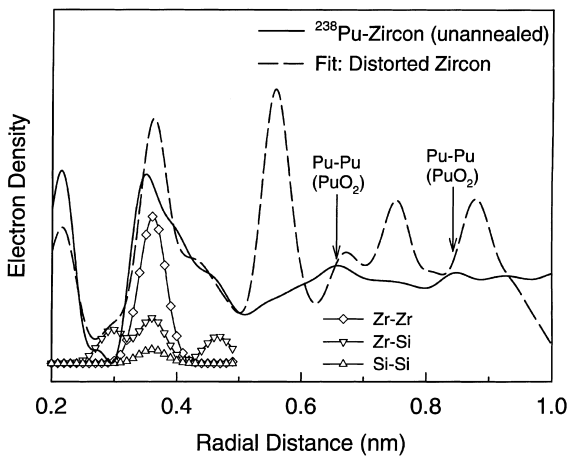

Fig. 6. PDF plot from amorphous (unannealed) ^{238}Pu-substituted zircon, including a fit to the data based on crystalline zircon to which a broadening term has been applied to account for lattice distortion. The detailed fit shows the contributions from the various cation–cation interactions out to 0.5 nm. Two minor peaks that coincide with the Pu–Pu distances in PuO_2 are indicated.

results are shown in Table 3. A comparison of the fitting results with the $PuSiO_4$ standard [22] indicates that all the cation–cation pairings present in the Pu end-member zircon are present in this nominally amorphous ^{238}Pu-substituted zircon out to a distance of ~0.5 nm, in agreement with the PDF result. No evidence for either amorphous Pu-bearing second phases or Pu clustering within the zircon was indicated by the Pu L_{III}-edge EXAFS data. Notable distortion was, however, present through the reduction in the number of the atom pairs, the presence of only one Pu–O distance at ~0.23 nm, compared to the two in $PuSiO_4$, and the contraction of the Pu–Zr distance to ~0.36 nm as indicated from the PDF. However, despite the loss of long-range crystallinity through the significant accumulation of α-decay damage, the local Pu environment out to ~0.5 nm remains well described by $PuSiO_4$ and consequently is remarkably similar to the Pu environment in the crystalline ^{239}Pu-substituted zircon described in Table 2. Further, the retention of a distorted zircon structure around the Pu indicates that the zircon stoichiometry has been retained on the atomic level in the amorphous ^{238}Pu-substituted zircon, similar to results reported for natural metamict zircons [12,23].

The fitting results from the Zr K-edge EXAFS from the unannealed ^{238}Pu-substituted zircon are shown in Table 4, along with reference distances for crystalline zircon [21] and monoclinic ZrO_2 [25]. A number of structural deviations exist, including the presence of a single Zr–O distance at ~0.22 nm, which is the average of the two Zr–O distances in crystalline zircon. The presence of two separate Zr–Zr distances relative to a single ~0.366 nm distance in the crystalline zircon and the loss of observable Zr–Si correlations, as mentioned previously, are both indicative of the level of distortion in the zircon structure.

Clearly, the Zr sub-lattice has been significantly impacted by the accumulated α-decay damage. Care needs to be taken however before interpreting the Zr K-edge EXAFS results as evidence for phase separation in the amorphous material, as has been recently proposed [26,27]. The loss of observable Zr–Si correlations on the Zr sub-lattice does not imply the diffusion of Zr and Si to form zirconia-rich and silica-rich microdomains. Indeed the significant discrepancies between the Zr K-edge fitting results from the amorphous ^{238}Pu-substituted zircon and monoclinic ZrO_2 do not support this conclusion, and other researchers [12,23] reported no evidence for decomposition into component oxides in natural metamict zircons. Further, if significant cation diffusion were to occur during the cooling of α-recoil cascades as claimed [27], then it should be equally evident for the Pu environment and not merely restricted to the Zr environment.

Table 3
Pu L_{III}-edge EXAFS fitting results from the unannealed ^{238}Pu-substituted zircon, along with reference data from $PuSiO_4$ [22]

	Shells	Pu–O	Pu–O	Pu–Si	Pu–Zr	Pu–Si	Pu–Si
^{238}Pu-zircon	Distance (nm)	0.232 (4)	–	0.316 (3)	0.360	0.383	0.443
	Number	5 (1)	–	1.7 (5)	1.3 (4)	0.9 (3)	3 (1)
	ΔSigma	0.17 (2)	–	0.11 (2)	0.10 (1)	0.11 (2)	0.16 (2)
	Shells	Pu–O	Pu–O	Pu–Si	Pu–Si/Zr	Pu–O	Pu–Si
$PuSiO_4$	Distance (nm)	0.229	0.249	0.311	0.378	0.421	0.488

Table 4
Zr K-edge EXAFS fitting results from the ^{238}Pu-substituted zircon, along with reference data from $ZrSiO_4$ [21] and monoclinic ZrO_2 [25]

	Shells	Zr–O		Zr–Zr	Zr–Zr
^{238}Pu-zircon	Distance (nm)	0.216 (3)		0.332 (2)	0.408 (2)
	Number	4 (1)		4 (1)	2.8 (9)
	Δ Sigma	0.13 (2)		0.13	0.13
	Shells	Zr–O	Zr–O	Zr–Si	Zr–Si/Zr
$ZrSiO_4$	Distance (nm)	0.213	0.227	0.299	0.366
	Number	4	4	2	4/4
	Shells	Zr–O	Zr–O	Zr–Zr	Zr–Zr
ZrO_2 (M)	Distance (nm)	0.210 (7)	0.223 (3)	0.346 (12)	0.391
	Number	4	3	7	2

The failure to observe Zr–Si correlations in amorphous zircon may be explained in terms of irregular rotation of the Zr and Si polyhedra with respect to each other, as discussed above. This would serve to destroy the unique Zr–Si distances present in crystalline zircon, and consequently prevent them from being observed by EXAFS. This is consistent with the Raman spectroscopy results [28] that indicate the SiO_4 tetrahedra remain as relatively stable structural units in extremely metamict zircons but are tilted relative to each other, although there was no evidence for increased polymerization of the SiO_4 tetrahedra. Such a structural rearrangement could also possibly explain the presence of two Zr–Zr distances, whose average distance is consistent with the single Zr–Zr distance in crystalline zircon. More importantly, this would preserve the zircon stoichiometry on the atomic scale, as required from the Pu L_{III}-edge EXAFS results.

Self-radiation damage from the accumulated dose of 2.8×10^{19} α-decays/g in this ^{238}Pu-substituted zircon has clearly resulted in the loss of long-range order and formation of an amorphous structure for length scales greater than 0.5 nm. Both the PDF and EXAFS results are consistent with the interpretation of loss of long-range order, but one in which a distorted zircon structure, consisting of SiO_4 and ZrO_8 polyhedra rotated relative to each other, is retained over length scales of up to 0.5 nm. These observations preclude the decomposition of zircon into component oxides as a result of self-radiation damage.

3.3. ^{238}Pu-substituted zircon annealed at 1000°C for 12 h

Annealing the amorphous ^{238}Pu-substituted zircon at 1000°C for 12 h in air resulted in complete oxidation of the Pu^{3+} to Pu^{4+} and the crystallization of zircon's constituent oxides. The XRD pattern for this sample is shown in Fig. 7, along with a diffraction pattern taken from an empty Kapton holder. The multiple-layer Kapton holder required to contain these radioactive samples is responsible for the significant non-linear background present in the diffraction pattern from the annealed zircon. The positions of the principal PuO_2 peaks have been marked in Fig. 7, along with the main SiO_2 peak; the remaining, slightly broad, diffraction peaks are from ZrO_2. The coincidence of the main SiO_2 peak with the main $ZrSiO_4$ reflection precludes a definitive statement regarding the complete absence of any zircon based on this single peak. Detailed fitting of the broad ZrO_2 diffraction maxima revealed that both the tetragonal and cubic forms are present. The lattice parameter from the cubic PuO_2 is 0.5388 nm, which is considerably smaller than the 0.53960 nm reported for pure PuO_2 [29], suggesting that the PuO_2 may contain a proportion of ZrO_2 in solid solution. As indicated in Table 1, the ionic radius of Zr^{4+} is smaller than that of

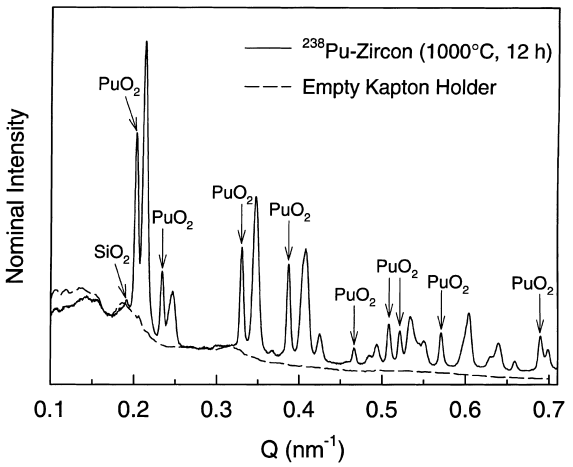

Fig. 7. XRD pattern from the ^{238}Pu-substituted zircon annealed at 1000°C for 12 h in air, along with a scan from an empty Kapton holder (dotted line). The major PuO_2 and SiO_2 lines are indicated, all other reflections are from a mixture of cubic and tetragonal ZrO_2.

Pu^{4+}, which would account for the lattice contraction observed for a $(Pu, Zr)O_2$ solid solution relative to PuO_2. No evidence of diffuse scattering that may be attributed to any residual amorphous material was found in the diffraction pattern, although X-ray scattering experiments are more sensitive to heavier elements and the presence of amorphous SiO_2 would be difficult to detect.

The PDF data obtained from this diffraction pattern are shown in Fig. 8, together with a fit based on a mixture of cubic and tetragonal ZrO_2, PuO_2 and SiO_2.

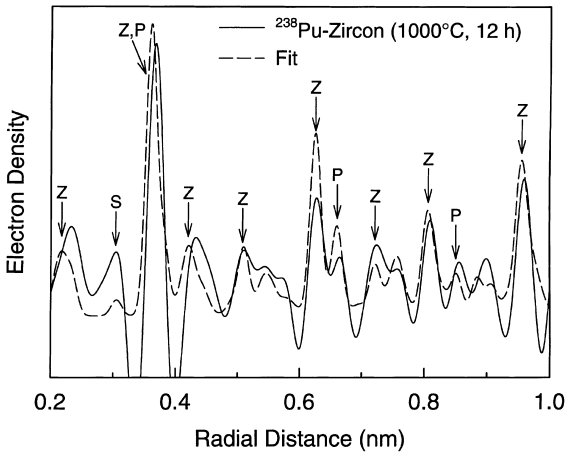

Fig. 8. PDF plot from the ^{238}Pu-substituted zircon annealed at 1000°C for 12 h in air, including a fit to the data based on the crystalline component oxides of zircon. Major contributions to the total PDF from ZrO_2 (cubic or tetragonal), PuO_2 and SiO_2 are marked by Z, P and S, respectively.

Table 5
Pu L_{III}-edge EXAFS fitting results from the ^{238}Pu-substituted zircon annealed at 1000°C for 12 h, along with reference data for PuO_2 [29]

	Shells	Pu–O	Pu–O	Pu–Si	Pu–Si	Pu–Pu	Pu–Zr
^{238}Pu-zircon	Distance (nm)	0.219 (2)	0.236 (2)	0.307 (2)	0.345 (2)	0.380 (1)	0.476 (1)
1000°C/12 h	Number	5 (1)	6 (1)	2.0 (6)	5 (1)	5 (1)	4 (1)
	Δ Sigma	0.00 (4)	0.00 (4)	0.09 (2)	0.06 (2)	0.00 (3)	0.07 (1)

	Shells	Pu–O	Pu–Pu
PuO_2	Distance (nm)	0.234	0.382
	Number	8	12

Table 6
Zr K-edge EXAFS fitting results from the ^{238}Pu-substituted zircon annealed at 1000°C for 12 h, along with reference data for tetragonal ZrO_2 [30]

	Shells	Zr–O	Zr–O	Zr–Zr	Zr–Zr	Zr–Zr	Zr–Zr
^{238}Pu-zircon	Distance (nm)	0.209 (2)	0.235 (2)	0.364 (1)	0.516 (2)	0.717 (2)	0.872 (1)
1000°C/12 h	Number	3.5 (9)	1.9 (6)	9 (2)	3 (1)	14 (4)	6 (2)
	Δ Sigma	0.07 (2)	0.07 (2)	0.06 (1)	0.07 (1)	0.09 (1)	0.06 (1)
ZrO_2 (T)	Distance (nm)	0.210	0.236	0.36–0.363	0.51–0.518	0.72–0.726	0.887
	Number	4	4	12	6	12	8

While the fit to the data is not perfect, all the major features have been accounted for. When combined with the narrow and clearly defined XRD features in Fig. 7, the results exclude the presence of significant residual amorphous material.

As expected, PuO_2 dominated the Pu L_{III}-edge EXAFS from this ^{238}Pu-substituted zircon annealed at 1000°C, as shown in Table 5. Significantly, the weak Pu–Si correlations observed at ~0.3 and 0.35 nm are consistent with the presence of some Pu in zircon. Given the crystalline nature of the sample and the minor peak in the region of the main zircon peak, the observed Pu–Si correlations are consistent with the onset of some recrystallization of zircon. Tetragonal ZrO_2 dominated the Zr K-edge EXAFS, as illustrated by the results and literature data [30] given in Table 6. Apart from the split Zr–O distances, it is very difficult to separate cubic and tetragonal ZrO_2 based on the fitting results.

To summarize, annealing the ^{238}Pu-substituted zircon at 1000°C for 12 h in air appears to have resulted in the complete crystallization of the zircon's constituent oxides, as well as the presence of a small amount of Pu-zircon. This was quite unexpected in light of the previous isochronal step-annealing study carried out on this material at approximately half the current dose [3,5,6], in which the onset of minor ZrO_2 crystallization was observed only at temperatures between 1050°C and 1200°C. In the case of natural metamict zircons, where the level of damage (i.e., accumulated dose and amount of residual crystallinity) may vary between samples, isochronal step-annealing over this same temperature range results in the formation of ZrO_2 in highly metamict zircon [11] or no ZrO_2 in partially metamict zircon [15]. These results suggest that the decomposition into component oxides may depend on both the initial amorphous or metamict state (partially or fully amorphous) and the structural evolution during isochronal step-annealing.

3.4. ^{238}Pu-substituted zircon annealed at 1200°C for 12 h

Based on the results at 1000°C, it is not surprising that annealing the amorphous ^{238}Pu-substituted zircon at 1200°C for 12 h in air results not only in the complete oxidation of the Pu^{3+} to Pu^{4+} but also in the complete recrystallization of the zircon structure, along with some PuO_2, as shown in Fig. 9. No evidence for a residual amorphous component was present in the diffraction pattern, so the zircon had been fully recrystallized by annealing at a temperature, some 250°C lower than previously reported [3,5,6].

The lattice parameters obtained from the ^{238}Pu-substituted zircon annealed at 1200°C for 12 h in air are listed in Table 7. An estimate of the amount of Pu present in the zircon, based on the measured lattice parameters in the manner described above, would be between 65% and 70% of the original 0.08 formula units depending on the factor used. The recrystallized ^{238}Pu-substituted zircon would therefore appear to contain more Pu than the annealed crystalline ^{239}Pu-substituted zircon.

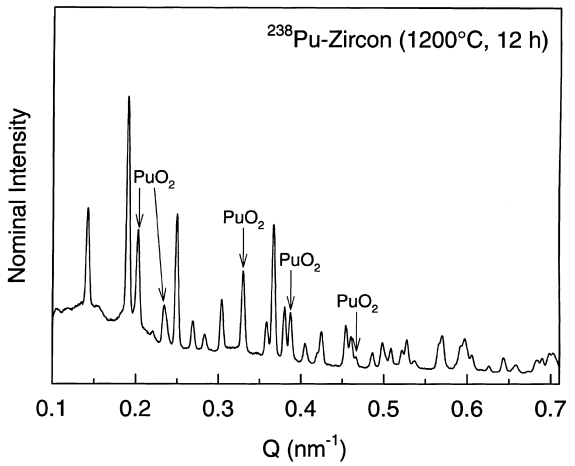

Fig. 9. XRD pattern from the ^{238}Pu-substituted zircon annealed at 1200°C for 12 h in air. The major PuO_2 lines are indicated. All other reflections are from zircon.

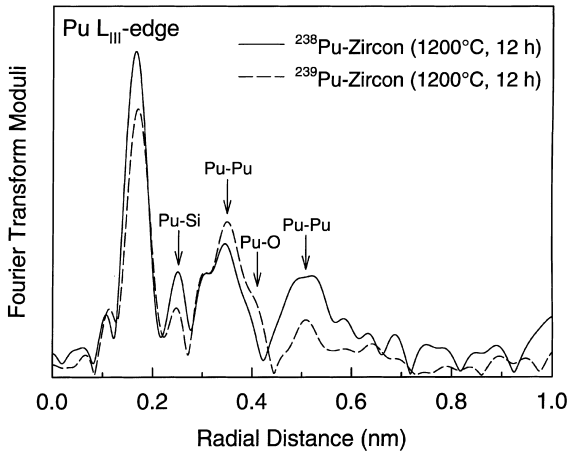

Fig. 10. Comparison of the Fourier transforms of the Pu L_{III}-edge EXAFS taken from the ^{238}Pu- and ^{239}Pu-substituted zircons after annealing in air at 1200°C for 12 h. Note that peaks in the Fourier transform have not been corrected for phase shift and as a result appear 0.05–0.10 nm shorter than fitted values.

Table 7
A comparison of the unit cell volumes obtained from the ^{238}Pu-substituted zircon annealed at 1200°C for 12 h in air with those for a reference zircon [21]

	^{238}Pu-zircon 1200°C/12 h	$ZrSiO_4$
Cell volume (nm^3)	0.2631	0.2608
Δ rel. $ZrSiO_4$	+0.0023	0
Pu valence	+4	–
Ionic size (nm)	0.086 (Pu)	0.072 (Zr)
% Pu in zircon	65%	0%

A comparison of the Fourier transforms of the Pu L_{III}-edge EXAFS taken from the ^{238}Pu- and ^{239}Pu-substituted zircons heated at 1200°C for 12 h is shown in Fig. 10. The intensity of the transform modulus for the annealed ^{238}Pu-substituted zircon is greater than from the annealed ^{239}Pu-substituted zircon over all distances apart from where the distinguishable PuO_2 distances reside. This is consistent with the 1200°C annealed ^{238}Pu-substituted zircon containing a greater proportion of Pu in the zircon lattice than the annealed crystalline ^{239}Pu-substituted zircon. The strong contribution from the annealed ^{238}Pu-substituted zircon at ~0.5 nm is consistent with the large Pu–Zr correlations for zircon in this region. These are significantly weaker in the annealed ^{239}Pu-substituted zircon, whose structure is dominated by the contributions from PuO_2.

A comparison of the Zr K-edge Fourier transforms from the ^{238}Pu- and ^{239}Pu-substituted zircons annealed at 1200°C is shown in Fig. 11. Excellent agreement exists in both the shape and width of the transform features out to 1 nm. While intensity variations are present, the

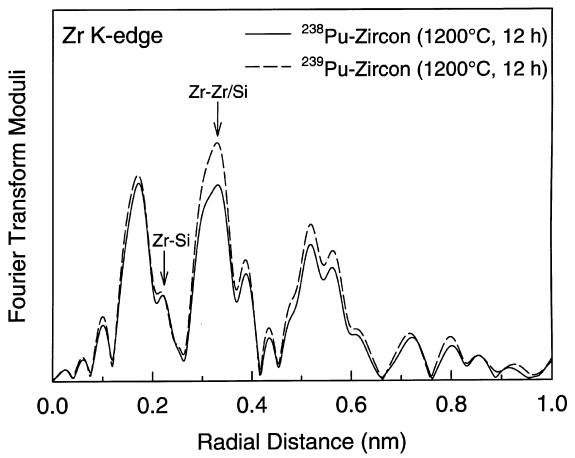

Fig. 11. Comparison of the Fourier transforms of the Zr K-edge EXAFS taken from the ^{238}Pu-and ^{239}Pu-substituted zircons after annealing in air at 1200°C for 12 h. Note that peaks in the Fourier transform have not been corrected for phase shift and as a result appear 0.05–0.10 nm shorter than fitted values.

equivalent shape and width of the transform features indicates that the local Zr environments in these two samples are comparable. No evidence for any residual amorphous material in the ^{238}Pu-substituted zircon annealed at 1200°C is evident based on the structure of the Zr sub-lattice.

The equivalency of the Zr environments observed in the ^{238}Pu-substituted zircon annealed at 1200°C with those in both ^{239}Pu-substituted zircons annealed at 1200°C (Fig. 11) and reference zircon [21] (Table 8) is consistent with the recrystallization of the amorphous

Table 8
Zr K-edge EXAFS fitting results from the ^{238}Pu-substituted zircon annealed at 1200°C for 12 h in air, along with reference data for $ZrSiO_4$ [21]

	Shells	Zr–O		Zr–Si	Zr–Si/Zr	Zr–Si	Zr–Zr
^{238}Pu-zircon	Distance (nm)	0.216 (2)		0.301 (2)	0.364 (1)	0.469 (2)	0.557 (1)
1200°C/12 h	Number	8 (2)		1.6 (5)	1.6 (5)	3 (1)	6 (2)
	Δ Sigma	0.10 (2)		0.05 (2)	0.0	0.0	0.04 (2)
	Shells	Zr–O	Zr–O	Zr–Si	Zr–Si/Zr	Zr–Si	Zr–Zr
$ZrSiO_4$	Distance (nm)	0.213	0227	0.299	0.366	0.467	0.557
	Number	4	4	2	4/4	4	5

^{238}Pu-substituted zircon (at 1200°C) directly from the amorphous state and not via the formation of oxide intermediaries. Further insight is provided by the nature of the PuO_2 that forms during annealing at 1200°C. The PuO_2 exsolved from the crystalline ^{239}Pu-substituted zircon at 1200°C is expected to be pure and free of any ZrO_2. If the amorphous ^{238}Pu-substituted zircon annealed at 1200°C recrystallizes via the formation of oxide-intermediaries, the PuO_2 present in the annealed sample is expected to contain some ZrO_2, similar to that observed in the ^{238}Pu-substituted zircon annealed at 1000°C. However, if zircon recrystallizes directly from the amorphous state, the PuO_2 that forms is expected to be pure. The cubic PuO_2 lattice parameters from both the ^{238}Pu- and ^{239}Pu-substituted zircons are equivalent with pure PuO_2 [29], being 0.5400, 0.5393 and 0.5396 nm, respectively. This indicates that no ZrO_2 is present in the PuO_2, which suggests that zircon recrystallizes directly from the amorphous state at 1200°C. This deduction is also consistent with the previous annealing study of this material [3,5,6], where annealing at 1450° for 12 h was required to recrystallize the zircon structure because phase separation occurred at lower temperatures during the step-annealing process.

A comparison of the PDF data obtained from the XRD patterns taken from the ^{238}Pu- and ^{239}Pu-substituted zircons after their respective anneals at 1200°C for 12 h is shown in Fig. 12. Excellent structural agreement is evident between these two samples. The intensities of the Zr–Zr/Pu pairs in the annealed ^{238}Pu-substituted zircon, as indicated in Fig. 12, are generally more intense than in the annealed ^{239}Pu-substituted zircon, which is consistent with the incorporation of a greater proportion of Pu in the recrystallized ^{238}Pu-substituted zircon. No evidence for any residual amorphous material in the ^{238}Pu-substituted zircon annealed at 1200°C for 12 h in air is evident from the PDF data.

The ability on one hand to crystallize the constituent oxides of zircon at 1000°C, and on the other to fully recrystallize zircon at 1200°C, some 250°C lower than previously reported, is very unexpected and raises important questions as to how the current findings relate to the previous annealing studies discussed earlier. The

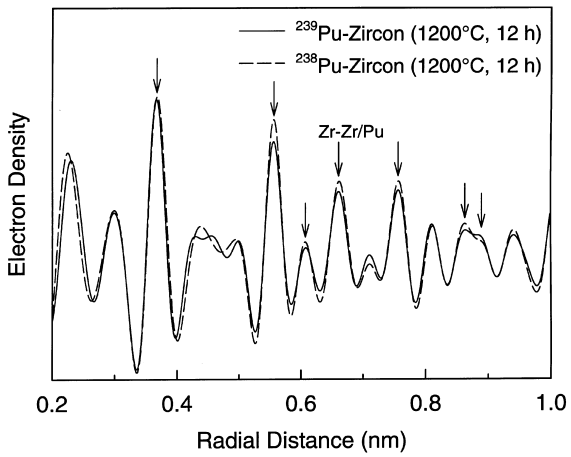

Fig. 12. A comparison of the PDF data from the ^{238}Pu- and ^{239}Pu-substituted zircons annealed at 1200°C for 12 h in air. The positions of the principal Zr–Zr/Pu pairs in the Pu-substituted zircons are indicated by arrows.

principal difference between the current study and previous studies is the manner in which the samples were annealed. In previous isochronal annealing studies of highly amorphous zircons [3,5,6,11], a single sample was sequentially heated to successively higher temperatures; whereas in the current study, separate samples were rapidly ramped (600°C/h) to the designated annealing temperature. In the previous study [3,5,6] of the amorphous ^{238}Pu-subsubstituted zircon, a two-stage recrystallization process, via the formation of oxide intermediaries between 1050°C and 1200°C, was observed, with complete recovery of the crystalline zircon structure at 1450°C. In the current study of the same material at a significantly higher dose, the amorphous state of the ^{238}Pu-substituted zircon is directly and fully recrystallized to the zircon structure at temperatures as low as 1200°C, but only because it is ramped rapidly to the annealing temperature. This suggests that rapid heating through the temperature regime where decomposition of the amorphous state to component oxides is observed can lead to congruent recrystallization of the zircon structure. However, if intermediate oxides are

allowed to form, then much higher annealing temperatures are required for recovery of the zircon crystal structure. It should be noted that in an isochronal annealing study of partially metamict zircons [15], which contained both amorphous and damaged-crystalline regimes, no intermediate formation of ZrO_2 was observed during recrystallization of the amorphous domains, and recovery of the crystalline zircon structure was complete at 900°C. Thus, structure evolution during annealing is not only dependent on the initial structural state and subsequent annealing temperature, but also on the heating rate and time at temperature. It is the interplay of the kinetics of various recovery and diffusion processes that control structural evolution during annealing.

One of the keys to understanding this behavior lies in characterizing the short-range structure of the amorphous state. The general inference from previous annealing studies [3,5,6,11], as illustrated in Fig. 1, is that during the isochronal step-anneals up to 900°C, where no significant recovery of density or recrystallization was observed, no significant change in the amorphous structure had occurred. However, the current results suggest that this is not the case. While no long-range order has developed, significant alteration to the short-range structure has probably occurred that impacts subsequent recrystallization behavior. Closer examination of the previous density recovery data (Fig. 1) indicates that some decrease in density occurs between 600°C and 900°C. This temperature range coincides with that where both increases in the mean Zr–O and Zr–Zr distances and an increase in Zr coordination number are observed in the EXAFS data for annealed metamict zircons [15]. Furthermore, perturbed angular correlation spectroscopy (PACS) data [17] show that local ordering occurs in metamict natural zircons for annealing above 600°C. Thus, the initial amorphous structure of zircon, which is devoid of long-range order but retains a distorted zircon structure and stoichiometry over length scales up to 0.5 nm, begins short-range structural evolution at temperatures above 600°C. This onset of short-range structural changes precedes the decomposition into component oxides observed in the isochronal step-annealing studies [3,5,6,11] and may precede the decomposition observed for the rapid-ramp annealing at 1000°C in the current study. The key to the direct recrystallization of amorphous zircon at 1200°C is rapidly heating the sample through the temperature range where decomposition is apparently energetically favored. The question that remains unanswered is "why is decomposition into component oxides favored over recrystallization of the zircon structure at low temperatures?"

Both step-annealing and rapid-ramp annealing at temperatures below 1200°C appear to result in the decomposition of amorphous zircon into component oxides (crystalline ZrO_2 and amorphous SiO_2). This implies that the distorted zircon structure and stoichiometry that is evident in the amorphous structure at room temperature is lost during structural evolution at intermediate temperatures. The phase separation associated with the observed decomposition implies sufficient cation diffusion for nucleation and growth of ZrO_2, which implies that the decomposition will be kinetically limited. Thus, as observed, rapid heating to higher temperatures can negate such decomposition. However, this does not answer the question as to why the amorphous structure will preferentially decompose rather than recrystallize, particularly since the local composition and structure is that of distorted zircon.

Both the decomposed constituent oxide structure and the recrystallized zircon structure represent lower energy states than the amorphous state [16], with crystalline zircon being the lowest energy state in the temperature range of this study. Consequently, there is an energetic driving force for both structural rearrangements; however, there is apparently a lower energy barrier for decomposition (i.e., cation diffusion) than for recrystallization of the zircon structure. Since the SiO_4 tetrahedra geometry is stable in metamict zircon [28] and is almost temperature independent in zircon [31], most short-range structural changes with increasing temperature are associated with observed increases in both Zr–O distances and Zr coordination, which may affect or enhance Zr diffusion. Although tetravalent cation self-diffusion in crystalline zircon has exceedingly high activation energies (~8 eV) [32,33], this is largely due to the very high formation energy for the Zr vacancy, as discussed in a recent computer simulation study [34] that determined the migration energy for the Zr vacancy to be 1.2–1.4 eV in crystalline zircon. Consequently, in highly damaged or amorphous zircon, where there is an existing high concentration of Zr vacancies or where vacancy formation energies may be considerably reduced, self-diffusion may be activated at lower temperatures. One might further speculate that the increase in Zr–O distances with temperature may increase the mobility of Zr in the amorphous zircon structure, particularly while the coordination number is still less than eight. This provides some explanation for the observed preferential decomposition of amorphous zircon to constituent oxides via Zr cation diffusion at intermediate temperatures. The implication is that the energy barrier for recrystallization of zircon is higher than for Zr self-diffusion in the amorphous state. Some insight into this is provided by the work of Mursic and coworkers [14], who observed that recrystallization of the zircon structure occurs in a temperature range where the sudden expansion of the Si–O bond and SiO_4 tetrahedral volume allows a Zr–O polyhedral subunit to rotate causing a structural relaxation. From the results discussed in this paper, the energy barrier for rotation of the Zr–O polyhedra must obviously be larger than the energy barrier for Zr self-diffusion in the amorphous state.

Future computer simulations may provide a means to confirm these observations.

4. Conclusions

The oxidation of Pu^{3+} to Pu^{4+} in the crystalline ^{239}Pu-substituted zircon results in a significant decrease in lattice distortion due to the reduction in ionic size mismatch between the Pu^{3+} and Pu^{4+} on the Zr^{4+} site. The nature of the first Zr–Si correlation in zircon is very sensitive to the level of lattice distortion present in the zircon. In addition, a significant amount of PuO_2 is exsolved from the zircon lattice after heating at 1200°C in air. Detailed characterization of the amorphous ^{238}Pu-substituted zircon is consistent with the loss of both long-range order and edge-sharing relationships between SiO_4 and ZrO_8 polyhedra. However, the amorphous state retains a distorted zircon structure and stoichiometry, consisting of SiO_4 and ZrO_8 polyhedra rotated relative to each other, over length scales of up to 0.5 nm. The recrystallization of the amorphous ^{238}Pu-substituted zircon could be achieved directly at temperatures as low as 1200°C if heated rapidly through the intermediate temperature regime where decomposition to oxides is preferred. The decomposition of amorphous zircon to constituent oxides is probably kinetically limited by Zr diffusion, which has a lower energy barrier than the polyhedral rotation required for recrystallization of the zircon structure from the amorphous state.

Acknowledgements

This study was supported by the Environmental Management Science Program, Office of Environmental Management, US Department of Energy under Contract DE-AC06-76RLO 1830. The XAS and XRD experiments were conducted at the Stanford Synchrotron Radiation Laboratory, which is supported by Office of Basic Energy Sciences, US Department of Energy. The assistance of the Seaborg Institute for Transactinium Science at Los Alamos National Laboratory in providing Health Physics and other experimental support is gratefully acknowledged.

References

[1] R.C. Ewing, W.J. Weber, F.W. Clinard Jr., Progr. Nucl. Energy 29 (2) (1995) 63.
[2] W.J. Weber, R.C. Ewing, C.R.A. Catlow, T. Diaz de la Rubia, L.W. Hobbs, C. Kinoshita, Hj. Matzke, A.T. Motta, M. Natasi, E.K.H. Salje, E.R. Vance, S.J. Zinkle, J. Mater. Res. 13 (1998) 1434.
[3] W.J. Weber, J. Mater. Res. 5 (1990) 147.
[4] T. Murakama, B.C. Chakoumakos, R.C. Ewing, G.R. Lumpkin, W.J. Weber, J. Am. Mineral. 76 (1991) 1510.
[5] W.J. Weber, J. Am. Ceram. Soc. 76 (1993) 1729.
[6] W.J. Weber, R.C. Ewing, L.M. Wang, J. Mater. Res. 9 (1994) 688.
[7] N.J. Hess, W.J. Weber, S.D. Conradson, J. Nucl. Mater. 254 (1998) 175.
[8] N.J. Hess, W.J. Weber, S.D. Conradson, J. Alloys Comp. 271–273 (1998) 240.
[9] R.D. Shannon, Acta Crystallogr. B 25 (1969) 925.
[10] R.E. Williford, B.D. Begg, W.J. Weber, N.J. Hess, this issue, p. 207.
[11] E.R. Vance, B.W. Anderson, Mineral. Mag. 38 (1972) 605.
[12] R.L. Barinsky, I.M. Kulikova, Phys. Chem. Miner. 1 (1977) 325.
[13] I. Nakai, J. Akimoto, M. Imafuku, R. Miyawaki, Y. Sugitani, K. Koto, Phys. Chem. Miner. 15 (1987) 113.
[14] Z. Mursic, T. Vogt, H. Boysen, F. Frey, J. Appl. Crystallogr. 25 (1992) 519.
[15] F. Farges, Phys. Chem. Miner. 20 (1994) 504.
[16] S. Ellsworth, A. Navrotsky, R.C. Ewing, Phys. Chem. Minerals 21 (1994) 140.
[17] H. Jaeger, L. Abu-Radad, D.J. Wick, Appl. Radiat. Isot. 48 (1997) 1083.
[18] E.R. Vance, B.W. Anderson, Mineral. Mag. 38 (1972) 721.
[19] D.A. Dimitrov, A.L. Ankudinov, A.R. Bishop, S.D. Conradson, Phys. Rev. B 58 (1998) 14227.
[20] H.P. Klug, L.E. Alexander, X-ray Diffraction Procedures for Polycrystalline and Amorphous Materials, Wiley, New York, 1974, p. 791.
[21] Powder Diffraction File PDF-2 Database, PDF 6-266, JCPDS-ICDD, 1998.
[22] C. Keller, Nukleonik 5 (1963) 41.
[23] F. Farges, G. Calas, Am. Mineral. 76 (1991) 60.
[24] F. Farges, R.C. Ewing, G.E. Brown Jr., J. Mater. Res. 8 (1993) 1983.
[25] R.E. Hann, P.R. Suitch, J.L. Pentecost, J. Am. Ceram. Soc. 68 (1985) 285.
[26] A.C. McLaren, J.D. Fitz Gerald, I.S. Williams, Geochim. Cosmochim. Acta 58 (1993) 993.
[27] A. Meldrum, S.J. Zinkle, L.A. Boatner, R.C. Ewing, Nature 395 (1998) 56.
[28] L. Nasdala, G. Irmer, D. Wolf, Eur. J. Mineral 7 (1995) 471.
[29] Powder Diffraction File PDF-2 Database, PDF 41-1170, JCPDS-ICDD, 1998.
[30] J.C. Howard, E.H. Kisi, R.B. Roberts, R.J. Hill, J. Am. Ceram. Soc. 73 (1990) 2828.
[31] R.M Hazen, L.W. Finger, Temperature, Pressure, Composition and the Variation of Crystal Structure, Wiley, New York, 1982, p. 231.
[32] D.J. Cherniak, J.M. Hanchar, E.B. Watson, Contrib. Minerol. Petrol. 127 (1997) 383.
[33] D.J. Cherniak, J.M. Hanchar, E.B. Watson, Chem. Geol. 134 (1997) 289.
[34] R.E. Williford, W.J. Weber, R. Devanathan, A.N. Cormack, J. Nucl. Mater. 273 (1999) 164.